Winter 12-17-2021

CHARACTERIZATION OF PHASE BEHAVIOR IN IDP SOLUTIONS BY UV-VIS SPECTROPHOTOMETRY AND PHASE VOLUME FRACTION MEASUREMENTS IN CAPILLARIES

Qing Sun

Qing Sun
Candidate

Biomedical Engineering
Department

This thesis is approved, and it is acceptable in quality and form for publication:

Approved by the Thesis Committee:

Nick J. Carroll , Chairperson

Gabriel P. López

Andrew P. Shreve

CHARACTERIZATION OF PHASE BEHAVIOR IN IDP SOLUTIONS BY UV-VIS SPECTROPHOTOMETRY AND PHASE VOLUME FRACTION MEASUREMENTS IN CAPILLARIES

by

QING SUN

BIOTECHNOLOGY, BACHELOR OF SCIENCE 2017

THESIS

Submitted in Partial Fulfillment of the

Requirements for the Degree of

MASTER OF SCIENCE

Biomedical Engineering

The University of New Mexico

Albuquerque, New Mexico

May, 2022

DEDICATION

In memory of my beloved grandfather, who was not able to see this full journey.

This thesis is dedicated to my parents, Litao Sun and Xulan Hao, who have always been there for me, and encouraged me to discover the universe.

ACKNOWLEDGMENTS

I heartily acknowledge Dr. Nick Carroll, my main advisor and mentor, whose innovative and divergent thinking has been guiding me and inspiring my unremitting exploration of science and my projects. I am very lucky and grateful to be able to work and explore the physical aspect of my research with him. Thank you for your immeasurable support and continuous funding throughout my research years.

I would like to also thank my co-advisor, Dr. Gabriel López, who put forward many critical directions and comments for my thesis, and taught me that attention to details and hard work are important components for good research. Thank you as well for the detailed comments and edits made to my writings, and the timely funding when I needed it.

To Dr. Andrew Shreve, my committee and instructor for my first class ever in the U.S. -- Thermodynamics, thank you for perceptive insights in the process of analyzing my data from the instrument, allowing me to re-summarize my conclusions.

Thanks again to all of my committee members, Dr. Carroll, Dr. López, and Dr. Shreve, for their patient guidance and wisest suggestions, which gave me a more comprehensive understanding of scientific research. Their guidance and professionalism will remain with me as I continue my career. To all my coworkers in Carroll López Lab and Brinker Lab, Adam Quintana, Telmo Díez Pérez, Ashley Tafoya, Dr. Jacqueline De Lora, Dr. Jimin Guo, Dr. Achraf Noureddine and others, thank you for all your knowledge, cares, supporting towards me, and all laughter and disasters our labs have been through to grow up as a whole.

To my friends, Caizhichao Zhang, Chenzi Dai, Peiyao Wu, and Haoshen Jiang, thank you for your unconditional support, patience, encouragement, and cherishable time we spent together during my studying abroad. And finally to my mom and dad, Xulan Hao and Litao Sun, your unconditional love made all of this possible.

CHARACTERIZATION OF PHASE BEHAVIOR IN IDP SOLUTIONS BY UV-VIS SPECTROPHOTOMETRY AND PHASE VOLUME FRACTION MEASUREMENTS IN CAPILLARIES

by

Qing Sun

B.A., Biotechnology, Beijing Normal University, Zhuhai, 2017

M.S., Biomedical Engineering, University of New Mexico, 2022

ABSTRACT

Intrinsically disordered proteins (IDPs) play vital roles in cell signaling and regulation by changing conformation dynamically under various stimulus. Thus, it is crucial to understand their physical properties in vitro especially liquid-liquid phase separation (LLPS). Here, we first used UV-vis spectrophotometry to investigate two of IDPs' physical properties – transition temperature (Tt) and coacervate size. This deeper insight allows us to further understand the dynamics of phase growth. We then constructed a binodal curve in the phase diagram by measurement of volume ratios in phase separated IDP solution in glass capillaries.

TABLE OF CONTENTS

LIST OF FIGURES

LIST OF TABLES

1. Chapter 1: Introduction

1.1. Liquid-liquid phase separation (LLPS) of polymer solutions

Liquid-liquid phase separation (LLPS) in polymer solutions and blends is a reversible process where a homogeneous single-phase solution separates into an inhomogeneous multi-phase solution. Phase separation is driven by a system's tendency to minimize free energy thermodynamically. A system's Gibbs free energy of mixing is given by $\Delta G_{mix} = \Delta H_{mix} - T\Delta S_{mix}$ where ΔH is the enthalpy of mixing and ΔS is the entropy of mixing. When $\Delta G_{mix} > 0$, phase separation will happen spontaneously to achieve the minimal free energy stage.[1] [2]. A de-mixed polymer solution usually consists of a polymer rich (condensed) phase and a dilute phase for a binary polymer solution.

A phase diagram is a plot shows phase boundaries made of phases formed in different polymer compositions over a range of temperatures.

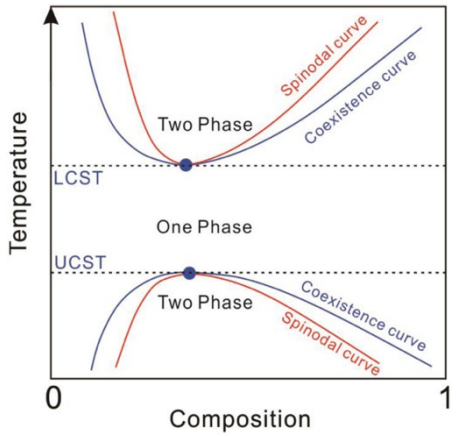

Figure 1 Binary solution phase diagram showing lower critical solution temperature (LCST) and upper critical solution temperature (UCST). UCST and LCST-type phase diagram shows temperature as a function of polymer volume fraction that is calculated from polymer concentration. Figure adapted from [3].

The boundary of the liquid-liquid phase separation is called the binodal. It separates the single-phase and two-phase regions[4]. The two-phase region again is divided

into an unstable region, bounded by the spinodal, and another meta-stable region of nucleation and growth between the spinodal line and the binodal line. In Figure 1, we observe a homogeneous solution in-between of the two binodal line, while liquid-liquid phase separation could take place above the binodal line or below at appropriate temperatures.

In a phase diagram, the point where two curves coincide is called the critical point. In a binary system at a critical point, depending on polymer property, polymer solutions may exhibit lower critical solution temperatures (LCST), upper critical solution temperatures (USCT), or a combination of both[5]. When a polymer solution exhibits an LCST, phase separation into polymer- and solvent-rich phases will take place at higher temperatures, whereas UCST systems show the opposite behavior.

There are two types of structure growth of phase separation, spinodal decomposition (SD) and nucleation and growth (NG), depending on the quenching temperature. Spinodal decomposition happens when the quenching temperature is located in the spinodal region at a given composition, where phase separation happens spontaneously. Spinodal decomposition starts with a large amount of growth of infinitesimal concentration fluctuations [6], and it is usually divided into three stages according to spatial concentration fluctuations in polymer solutions leading to a lower free energy of mixing [7]. These three stages, early-stage SD, intermediate-stage SD, and late-stage SD, both the amplitude of the concentration fluctuations and the wavelength of Fourier mode fluctuations grow over time until amplitude of the concentration fluctuations reaches to equilibrium while the wavelength (size) of the unmixed structure keeps growing. [8] Nucleation and growth occur when the quenching temperature locates

in the metastable region of the phase diagram. Phase separation happens only if the system has to overcome a barrier of activation, and by the formation of sufficient sized nucleation sites which are considered large concentration fluctuations[9].

1.2. Introduction of intrinsically disordered proteins (IDPs) and Elastin-like polypeptides (ELPs)

Many proteins or protein regions have been found lacking stable 3D or 2D structures in nature, especially in eukaryotes [10]. These structure-independent proteins are called intrinsically disordered proteins (IDPs), whereas some proteins contain both intrinsically disordered regions (IDRs) and structured regions. At the molecular level, IDPs and IDRs are not able to form stable, well-defined, globular 3D structures spontaneously. Even in cells, they are dynamically disordered and functionally complement ordered proteins in cellular signaling and regulation [11]. As a consequence, IDPs and IDRs' backbone Ramachandran angles have no specific equilibrium values and fluctuate rapidly through a range of conformations [12]. IDPs and IDRs can also undergo LLPS to form extended-disordered (random coils or pre-molten globules) or collapsed-disordered (molten globules) conformations that resemble non-native states of some globular proteins [13]. IDPs and IDRs usually have low complexity in their amino acid sequences, more significant proportions of charged and hydrophilic amino acids, and less hydrophobic amino acid proportions. These characters all contribute to the physical properties, which include phase separation in water with UCST or LCST behavior [14]. In conclusion, either a IDP solution exists UCST or LCST behavior depends on the content of hydrophobic versus polar/charged amino acids. Generally speaking, composition of

more hydrophobic amino acids is likely to have LCST behavior, while more aromatic amino acids and charged amino acids is likely to have UCST behavior[15].

IDPs and IDRs commonly exist in nature, and the more complex function that an organism has, the more abundant IDPs and IDRs it has [16]. According to some applications of various disorder predictors to proteomes, some predicted long IDRs (≥30 residues) are roughly the same level in bacteria and archaea. However, they are much more prevalent in eukaryotes with over half of eukaryotic proteins containing long predicted IDRs [17] [18]. This trend is related to the requirements for cell needs, especially cellular signaling. Most of the signal transduction proteins in eukaryotes contain disordered regions[19].

IDPs/IDRs frequently interact with multiple partners, and function as hubs in signaling, regulation, or control pathways. Their main functions are related with phase separation under stimulus and can be listed into four categories: molecular recognition, molecular assembly, protein modification, and entropic chain activities [20]. Those facts make IDPs play such vital roles and are strictly regulated in the cell [21], so IDP-mutations in conformation or sequence are associated with degradation of function and disease[22].

Predicting whether a protein is disordered and its characterization becomes very helpful for many investigations of protein-degradation-disease and disordered protein application structural designs. Several web servers can be used to predict protein disorder based on sequence analysis, and there are also databases containing predictions of common disordered proteins encoded from the human genome. Web servers such as The DisProt Predictor of Protein Disorder (DisProt)[23] and Prediction of Intrinsically Unstructured Proteins (IUPred) [24]. There are also databases, such as the Database of

Disordered Protein Prediction (D2P2), containing the compilation of predictors stated above and their algorithms [25].

Elastin is a type of extracellular matrix (ECM) protein, and it has approximately 800 amino acids and a MW of 68 kDa [26]. It has a highly hydrophobic domain and a crosslinking domain contains lysine, allowing elastin to extend and recoil repeatedly, and in the meantime crosslink with adjacent molecules [27]. Because of its unique physical properties, elastin mainly exists in large arteries, lung parenchyma, skin, and ligaments [28]. The soluble precursor of elastin is tropoelastin, which is secreted from cells during elastogenesis following by fibrils formation through enzymatically lysine crosslinking[29].

Elastin-like polypeptides (ELPs) are synthetic polypeptide biopolymers derived from the hydrophobic domain of tropoelastin and is composed of a form of $(VPGXG)_n$ pentapeptide repeating units [30]. The guest residue X can be any amino acid except proline, and n indicates the number of pentapeptide repeats in ELPs [31] [32]. Glycine (G) and proline (P) are essential in the ELPs' polypeptide backbone to contribute to the highly disordered structural properties of ELP molecules. The presence of glycine promotes the chain mobility of ELPs and further allows ELPs to form different chain conformations; the presence of proline enhances the rigidity and prevents ELPs from forming a stable secondary structure [33]. Other forms of ELPs can also be found as repetitive pentapeptides like KGGVG, heptapeptides, or nonapeptides; these ELPs show properties like elastin as well [34].

ELPs have an LCST polymer phase behavior in water, which means, it has a high degree of conformational flexibility below its cloud-point transition temperature (Tt), and phase separates into a reversible insoluble coacervate phase above its Tt [35]. The Tt of

ELPs can be affected by different stimuli such as salt concentrations, pH, light, solvent types; and can be tuned at the design level by changing the chain length, guest residues, and fusions motifs [36] [37] [38]. By studying and designing the number and types of guest residues in ELPs, the transition temperature of ELPs can be precisely controlled. Urry et al. studied the specific effects of guest residues with various hydrophilicity on transition temperatures of ELPs. Among them, guest residues with low hydrophilicity reduce the Tt of ELPs [39].

Because of ELPs' unique physical properties, they have been developed for a wide range of applications in biomedical engineering in the last decades, focusing mainly on protein purification, drug delivery, and tissue engineering. Applications will be introduced in detail in later chapters.

In conclusion, it is critical to study an IDPs' physical properties in vitro to further understand irregular physical behavior in cells or to better utilize these unique properties in biodevices. In the last section, we mentioned some characteristics of IDP, such as low complexity, highly repeated; ELPs are an extreme example of IDPs. They contain so much repeats of such short oligopeptide, so we selected ELPs as the model of this research. We used two different ELP models denoted E1-80 and E3. E1-80 contains 80 repeats of VPGVG, and E3 contains eight repeats of $(VPGXG)_{10}$-GKG, where the guest residues are 80% V and 20% A. Protein sequences showed in detail in Table 1.

Name	Protein Sequence	MW
E1-80	MSKGPG-$(VPGVG)_{80}$	**33,497 Da**
E3	[(GVGVPGVGVPGAGVPGVGVPGVGVPGVGVPGVGVPGAG VPGVGVPGVGVPGVG)-GKG]$_8$	**36,135 Da**

Table 1 ELP amino acid sequences[40].

1.3. Specific Aims:

1.3.1. Specific Aim 1: Study of the effect of heat power input on ELP phase behavior

In specific aim 1, we studied the relationships between heat power input and two physical properties of ELPs --transition temperature (Tt) and coacervate size distribution. We used a multicell temperature-controlled Cary 300 UV-vis spectrophotometer to get turbidity profiles for E3 and E1-80. To control the heat power input, different temperature ramping speed was used to get to the desired temperature. Tt is defined as the maximum slope of phase transition, where onset transition temperature is defined as the start of spinodal decomposition. Both of them from different ramping speeds were then calculated from the output absorbance data. Size distribution of ELPs from various ramping rates were also analyzed from the stationary phase of absorbance curves. The detail will be discussed in Chapter 3.

1.3.2. Specific Aim 2: Obtain binodal curve in the phase diagram using capillary measurement

Binodal (coexistence) curve is generally measured using the peak autocorrelation function (ACF) by dynamic light scattering (DLS) by gradually increasing the temperature with a light-scattering spectrometer. In order to capture the most accurate coexistence temperature, the general temperature control interval is 0.1ºC and the waiting time at the same temperature needs to be long enough. Here, we developed a method to construct a binodal curve using capillaries to measure volume ratio after phase separation of ELPs. There are two different ELP compositions under a specific temperature above the cloud-point temperature in the binodal curve; the smaller one is ELP composition in

water-rich phase, and the larger one is ELP composition in coacervate-rich phase. We calculated these two compositions by solving the mass balance equation using the water-rich phase volume ratio (i.e., water-rich phase volume/overall volume) and coacervate-rich phase volume ratio we obtained from capillary measurements. The sum of these two phase volume ratios should be equivalent to one. An ELP binodal curve was constructed by acquiring compositions of two phases under different temperatures in a much less work intensive manner. The detail will be discussed in Chapter 4.

2. Chapter 2: Review of the Literature

As discussed in Chapter 1, the equilibrium thermodynamic phase diagram provides tools to interpret polymer solution phase behavior under constrained conditions to explore condensed phase polymer and solvent compositions. In this chapter, we report literature summarizing key contemporary methods for phase diagram construction of synthetic and biological polymers with a focus on binodal and spinodal curve measurements.

2.1. Review of methods for determination of phase diagrams of synthetic polymers

Schäfer-Soenen et al. used differential scanning calorimetry (DSC) as early as 1997 to analyze liquid−liquid demixing of a Poly(vinyl methyl ether) (PVME)/water system[41]. Measurements with DSC were performed at a scanning rate of 0.1 °C/min to measure the temperature at the onset of the endotherm which is considered as the demixing temperature (Td). In a separate set of measurements, the cloud point was determined by turbidimetry by measuring the transparency of the samples using the

transmitted light intensity. Tc was taken as the corresponding temperature first deviation of the transmitted light intensity from linearity. Both results were plotted out as a function of volume fraction as the spinodal curve in a phase diagram. The plots showed that the results obtained by calorimetry match well with the turbidimetry method. In a recent study, Lin et al. demonstrated the versatility of this method by using DSC to measure the spinodal curve for a solid-state polymer-drug system to investigate phase behavior of a specific drug–polymer[42].

To get the binodal curve for PVME/water system, Schäfer-Soenen et al. performed isothermal annealing at constant temperature on samples at concentrations corresponding to polymer volume percentages between 4% and 10%[43]. After all solutions separated into two transparent layers, the volume ratios of these two layers were calculated by a method described in Vandeweerdt's Ph.D. thesis[44]. Here, the compositions of coexisting polymer phases were inferred through measurements using an Abbé refractometer. A calibration refractive−concentration plot was constructed first between concentrations 0% and 50% to later determine the concentration from refractive indexes.

Another method centered on refractometry to measure binodal curves was described by Kurnik et al. [45] They developed a temperature modulated optical refractometry (TMOR) method which enhanced accuracy comparing to the previous visual cloud point method. Pluronic L35 solution phase behavior was measured from 10°C to 100 °C at a heating/cooling rate of 0.1 °C/s using computer-controlled thermo-optic oscillating refraction characterization. Monochromatic light at wavelength of 589 nm was used and the total reflection limit of the divergent beam incident on the sample

from the prism was measured. The refractive index (nD) as determined along the temperature rise (T °C) was plotted and temperatures at the characteristic peak were affirmed as the demixing temperature. The binodal coexistence curve then was constructed as the temperature of demixing versus Pluronic L35 composition (wt%).

Recently a method combining microfluidics and solvent evaporation has been developed to construct phase diagram by measurement of saturation concentrations[46]. First, samples at sub-critical concentrations are trapped inside a microfluidic "phase chip" and concentrated gradually by removing water by evaporation, osmosis, or extraction into the flowing oil phase[47]. Reduction of the sample volume inside the chamber will lead to an increase of sample concentration. Under a Zeiss LSM 800 confocal microscope, samples are observed in real-time until LLPS were observed. Concentration at which phase separate (saturation concentration) was then calculated using the volume difference between sample at phase separation and sample at starting point for a given starting sample concentration. Binodal curves for low-complexity domain of RNA-binding protein hnRNPA1 (A1-LCD), a sequence variant of the A1-LCD termed A1-LCD$^{+12D+7R}$ and Bovine serum albumin (BSA) were then established by this method.

2.2. Review of methods for determination of phase diagrams of biopolymers

2.2.1. Binodal determination of intrinsically disordered proteins (IDPs)

For many biopolymers such as IDPs, transition temperature, which is the temperature required for phase transition at a specific polymer concentration, are usually measured and used to estimate the binodal phase boundary for construction of polymer solution phase diagrams. There are, however, other techniques to construct phase diagrams. Dzuricky et al. used charged resilin-like IDP samples in glass capillaries

mounted on top of a linear-temperature-gradient microfluidic device[48]. Tt was measured by light scattering intensity after phase separation took place. A linear temperature gradient across capillaries was achieved by having a heating and cooling source at both ends of the microfluidic device. An image was taken and analyzed under dark-field microscopy. Poly(N-isopropyl acrylamide) and poly(ethylene oxide) were used as reference polymer solutions to determine temperature as a function of capillary length as their coexisting temperatures were determined using light scattering intensity methods. The temperature gradient was assumed to have a linear relationship between pixel positions of the two samples. The phase separated capillaries were then scanned to generate a normalized light scattering intensity.

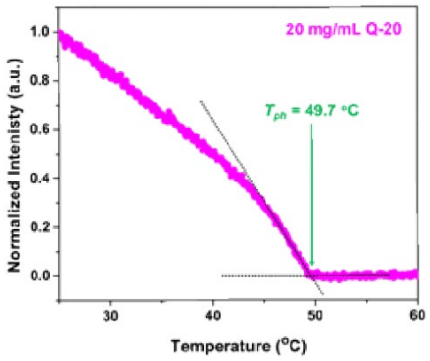

Figure 2 Line scan result of light scattering intensity as a function of temperature. The intersection of two dashed black lines represents Tph. Figure adapted from[49].

Phase transition temperature (Tph) was obtained from the plot normalized intensity versus temperature. Then binodal lines for different de novo designed artificial IDPs (A-IDPs) samples were established using multiple Tph at various concentrations from the temperature gradient device[50].

Tt can also be measured by observing LLPS under bright-field microscopy. Nott et al. used a sealed sample chamber for evaporation reduction with two coverslips and

IDP sample in between on top of their THMS600 thermal stage under microscope to observe LLPS of IDPs[51]. Photos were analyzed at every 50 seconds. Figure 3 shows an example of the determination of IDP transition temperature which is the temperature at the rapid change in standard deviation of pixel intensity marked at dashed line. Binodal curve was then constructed by collecting transition temperatures of a range of sample concentration.

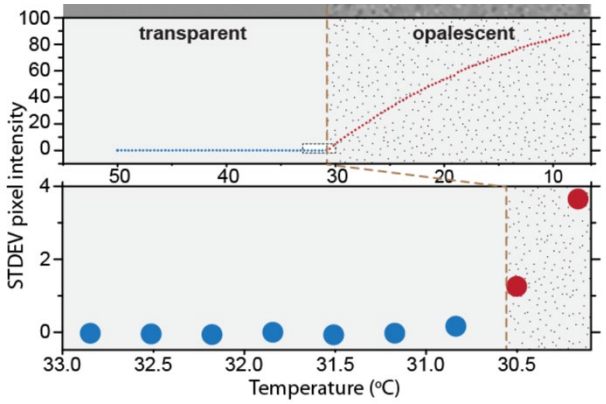

Figure 3 Determination of phase transition temperature by observation of sample transparency. Figure adapted from[52].

Similarly, Le et al. established a phase diagram of an IDP, Histidine-rich Beak Protein 2 (HBP-2), by observation of microdroplet conformational change and apparition of HBP-2 while raising temperature using optical microscopy to determine transition temperature for various sample concentrations[53].

2.2.2. Determination of phase diagrams of Elastin-like polypeptides (ELPs)

Light scattering is a common characterization technique used to determine LCST phase diagrams of ELPs. Pertinent to the work presented in this thesis, Simon et al. used dynamic light-scattering (DLS) and static light-scattering (SLS) measurements of the cationic LCST ELP protein known as E3 (for sequence see Table 1) to construct the binodal and spinodal curves of the equilibrium thermodynamic phase diagram. In this

work, akin to the methods described in previous sections to determine phase diagrams of synthetic polymers, light-scattering spectrometry was used to measure significant changes in DLS scattering autocorrelation functions (ACFs) at temperatures in 0.1°C increments to detect the onset of ELP phase separation to construct binodal curves. The corresponding temperatures at ACF peak changes for varying concentrations of ELP were recorded and plotted as a function of volume fraction.

The spinodal curve for E3 was calculated by first measuring the SLS intensity, I, at a single scattering angle of $\theta = \pi/2$, for E3 solutions at various temperatures and polymer concentrations well below the critical point. Next, reciprocal SLS intensity was plotted as a function of temperature for each polymer concentration sample. A representative 1/I versus T plot for a particular concentration of E3 is shown in Figure 4.

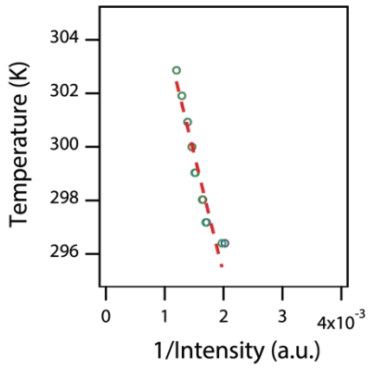

Figure 4 Plot of temperature versus the reciprocal value of SLS intensity (I) at a specific concentration for E3. Red dashed line indicates the best linear fit to experimental data points. Figure adapted from[54].

The spinodal temperature was determined from this plot as the temperature at which the extrapolated 1/I intersects with y-axis which corresponds to an infinite scattering intensity. Then the spinodal temperatures were plotted as a function of volume fractions as the spinodal curve of ELP solution[55].

Another method that is commonly used to characterize phase behavior and to determine estimates of binodal phase boundaries is temperature-dependent turbidimetry[56]. These measurements are usually carried out for ELPs by temperature-controlled UV-Vis spectrophotometry at a fixed wavelength of 350 nm[57]. Absorbance is measured while heating up samples at a preset temperature ramp rate. The transition temperatures are calculated as temperatures at the maximum in the first derivative of the absorbance with respect to temperature and are measured at various ELP compositions to rapidly create estimates of binodal phase diagrams[58 59 60].

3. Chapter 3: Investigation of observed ELP transition temperatures as influenced by heat power input using UV-vis spectroscopy

In this chapter, E1 (neutral charge) and E3 (cationic) solution turbidity measurements using a Cary 300 temperature-controllable UV-vis spectrophotometer are reported to characterize how heat power input, as described by an associated temperature ramp rate, influence measured transition temperatures as a function of ELP composition.

3.1. Introduction

3.1.1. Synopsis

In this study, we use canonical turbidity measurements to detect the transition temperatures of LCST ELPs because the incipient formation of coacervate drops will scatter light, and these events are easily detected by temperature-controlled UV-vis spectrophotometry. We measure turbidity using the commonly used temperature-controlled Cary 300 spectrophotometer (Agilent Technologies, Inc). The turbidity profile describes the absorbance of ELP solutions as a function of temperature. The transition

temperature (Tt) is defined as the midpoint of the sharp increase in turbidity, which is the temperature at the maximum first derivative of absorbance. In most reported studies, turbidity measurements are carried out at 1 ˚C/min temperature ramp rate[61 62 63]. We hypothesized that given phase separation has two types of kinetical morphology growth at compositions and temperatures that fall within the two phase envelope (nucleation and growth in the metastable regime or phase separation via spinodal decomposition), the use of different temperature ramping speeds of 2 ˚C/min, 1 ˚C/min, 0.5 ˚C/min, 0.25 ˚C/min, and 0.1 ˚C/min (and hence different power input) would have a measurable effect on both coacervate size distribution and the detected transition temperature.

3.1.2. Biomedical Applications of ELPs

Thermally responsive ELPs have been deployed within the biomedical field in mainly four areas: protein purification[64], biosensing[65], drug delivery[66], and tissue engineering[67]. The reversable LLPS capability of ELPs is exploited by a purification process called inverse transition cycling (ITC) to separate target protein from other proteins produced by the host cell[68]. Biosensing is another key field for ELPs owing to their responsiveness to environmental stimuli and associated visual readout brought on by conformational change of the polymers in solution. Stimuli such as Ph, light, and salt concentration can be used as triggers for ELPs to undergo LLPS[69]. A variety of molecules and polymers can be partnered with ELPs for drug delivery[70]. Additionally, ELPs can be modified to include cell targeting surfaces for uptake by certain cell types[71]. Since ELPs are derived from elastin, they are obvious scaffolds for tissue engineering with great controlled degradation or ligand presentation. ELPs have been used in regenerative medicine like tissue repair[72] and post-surgical wound healing[73]. Hence,

understanding the phase behavior of ELPs will have impact across a broad range of biomedical applications.

3.1.3. Temperature controlled UV-vis spectrophotometry for creation of ELP phase diagrams

Absorbance through UV-vis spectrophotometry investigates the interaction of light radiation with matter in the ultraviolet (200-400 nm) and visible (400-800 nm) range by measuring the amount of light transmitted through a sample as compared to a reference[74]. Absorbance (A) is calculated as $A = \log_{10}(\frac{I_0}{I}) = \varepsilon LC$ according to Beer–Lambert's law, where I_0 is the transmitted light amount; I is the original light amount; ε is absorption coefficient; L is the length of light path through sample; and C is concentration of the sample[75].

Transmitted light is first detected by the sensor and then analyzed and output light absorbance as a function of temperature by the computer. It has a low accuracy for measuring solution concentrations when absorbance values exceed 2 or 3. According to the equation above, an absorbance value of 1 implies that the sample absorbed 90% of the incoming light. Sometimes it is difficult for the detector to quantify small changes in the amount of light at the detector.

3.2. Methods

3.2.1. Materials

PBS was purchased from Alfa Aesar (Ward Hill, MA). Isopropyl β-D-1-thiogalactopyranoside (IPTG) was purchased from Amresco Inc. (Solon, OH). Terrific broth media powder was purchased from MO BIO laboratories Inc. (Carlsbad, CA). Paroline oil was purchased from Sigma Aldrich (St. Louis, MO). Syringe pumps were

purchased from Chemyx Inc. (Holliston, MA). Polyethylenimine (PEI) was purchased from Spectrum Inc. (New Brunswick, NJ). SDS-PAGE gel, Laemmli Sample Buffer, Coomassie Stains, SDS running buffer were purchased from Bio-Rad Laboratories Inc. (Hercules, CA).

3.2.2. Measurement instrument set-up

A Cary 300 UV-vis spectrophotometer (Agilent Technologies, Inc) was used to measure the turbidity profile of E1 and E3 solution samples at various ramp rates and polymer compositions. Before starting the program, we allowed the instrument to warm up for 2 hours for optimal results. In the Cary software, the program was set up as shown below in Figure 5.

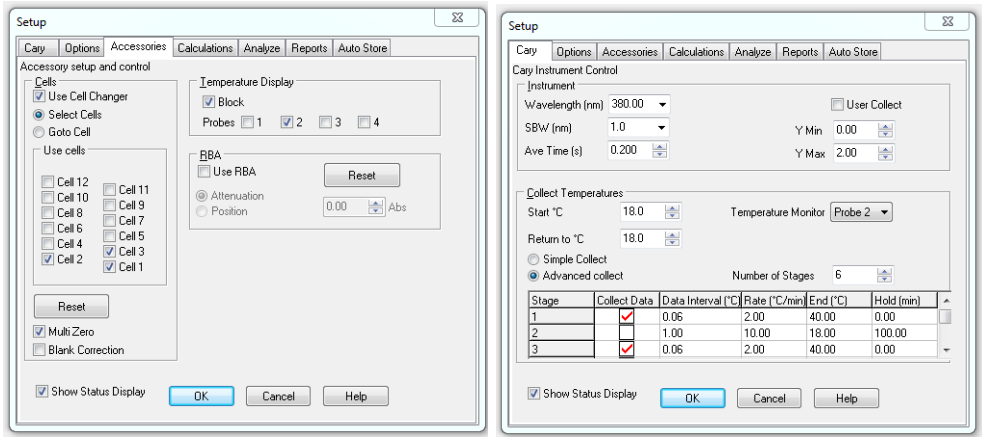

Figure 5 Setting pages of Cary measurements

Here, the *wavelength* was set to a common value typically used for ELPs, which are wavelengths between 350 nm to 380nm[76] [77]. The *averaging time* represents the time interval the instrument will average the absorbance data. The higher the averaging time is, the less the background noise shows, the smoother the signal is. Here, averaging times of 0.2 s, 0.5 s, 1 s, 1 s, and 2 s were used for ramping rates of 2 ˚C/min, 1 ˚C/min, 0.5 ˚C/min, 0.25 ˚C/min, and 0.1 ˚C/min, respectively. A temperature probe was submerged

into the sample for direct liquid temperature measurements, instead of block temperature measurements for more accurate real-time aqueous solution temperature readouts. The data collection time interval was set to be the minimal value of 0.06 ˚C/min, and ramping rates were set to be 2 ˚C/min, 1 ˚C/min, 0.5 ˚C/min, 0.25 ˚C/min, and 0.1 ˚C/min for each independent set of experiments. Between every repeat (3 repeats for each sample), a 100 min hold time at low temperature was set to allow the ELPs to redissolve into solution prior to the next set of measurements. Either multi zero or blank correction are appropriate selections to zero out the buffer before signal collection.

3.2.3. Experimental and ELP Synthesis Procedures

3.2.3.1. Protein expression and purification of E1-80 and E3

E3 was expressed in E. coli BL21(DE3) cell culture with antibiotic kanamycin, and cells were incubated under 37 ˚C at 200 rpm for 24 hours before harvest. Next day, cell culture was harvested by centrifugation under 3000 RPM for 10 min, then PBS was added to resuspend cell pellet. Sonification was then used to lyse cells on an ice bath by using program 10 sec on/20 sec off to avoid overheating cells for a total of 15 min per 40mL cell mix. Cell lysate should be slightly darker after sonification. It then was centrifuged at 4 ˚C for 10 mins to get rid of insoluble cellular lysate, subsequently adding 10% of polyethyleneimine (PEI) to get rid of nucleic acids by another centrifugation under cold. Then a method inverse transition cycling (ITC) that takes advantage of IDPs' physical properties is used to purify E3 cell lysate. It is triggered by centrifugation under temperature over 50 ˚C or by adding salt, resulting in aggregation of E3. Then the supernatant containing contaminating soluble molecules were discarded, and E3 is recovered by spinning the pellet with PBS overnight at 4 ˚C. There should be no pellet

after cold centrifugation after a few rounds of ITC. Then E3 was dialyzed against DI water using a MW 3500 dialysis cassette to remove excess salt overnight. 16-hour lyophilization then was performed for E3 for quantitively study.

E1-80 plasmid has a low complexity comparing to E3, so it is considered as a difficult template. For those proteins. A longer incubation time and additional of Isopropyl β- d-1-thiogalactopyranoside (IPTG) for cell culture is required.

Purified E3 and E1-80 were characterized by sodium dodecyl sulfate polyacrylamide gel electrophoresis (SDS-PAGE; BioRad, Inc.) under 180V for 40mins. Following electrophoresis, the gel was stained by Coomassie Brilliant Blue for 30 min. E180 is going to stain lightly than E3 because Coomassie Brilliant Blue interacts weakly with histidine or lysine or other aromatic residues[78]. After distaining for another hour, a picture was taken and showed as Figure 6. Figure 6 verifies the purity and sizes of E3 and E1-80 which respectively are 36kDa and 33.5kDa.

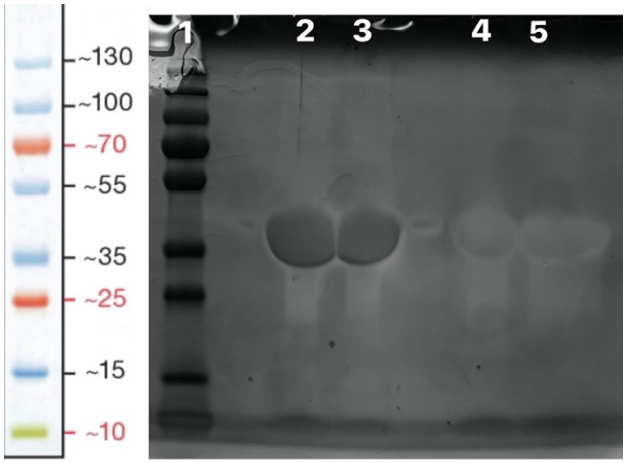

Figure 6 SDS-PAGE gel with ladder (1st lane), E3 (2nd and 3rd lanes), E1-80 (4th and 5th lanes).

3.2.3.2. Transition temperature detection using UV-vis spectrophotometry as a function of temperature ramp rate

Two concentrations of E3 and E1-80 in aqueous PBS buffer were prepared for Tt measurements under various heat power inputs, a high concentration of 1mM and a low concentration of 0.05 mM. Sample volumes of 100 μL were added to quartz cuvettes topped with 100 μL paroline oil to mitigate solvent evaporation during heating. A thermo senser was placed inside of solution samples to monitor the real-time temperature during heating. All measurements started at an initial temperature of 18 ˚C, and ran under five different temperature ramp rates of 2 ˚C/min, 1 ˚C/min, 0.5 ˚C/min, 0.25 ˚C/min, and 0.1 ˚C/min. All other relevant instrument settings are described in the Cary 300 UV-vis spectrophotometer set-up section 3.2.2. Absorbance was measured by the detector during temperature ramping, and then was processed and presented as a function of temperature in real-time. Measurements and heating are terminated when absorbance researched a stationary plateau value and each sample was returned to 18 ˚C. Each concentration has three duplicons, and each duplicon was measured three times to ensure repetitive data sets.

3.3. Data Analysis

3.3.1. Plot Absorbance (Abs) as a function of Temperature (T)

The absorbance data was then saved as .cvs file and analyzed and plotted using Excel scatter plot. Error bars were calculated using standard deviation from three repeats of three duplicons (i.e., nine data points for each sample measured).

3.3.2. Estimate of ELP transition temperature (Tt) using the maximum of first derivative of the absorbance

A sigmoidal curve in Python was fit to the absorbance data using the function curv_fit from SciPy, which is an open-source Python library. The Tt for each ELP sample was calculated by reporting the temperature with the maximum first derivative of absorbance, which is also the midpoint of the logarithmic growth phase. Another onset transition temperature was calculated by the first Tt is the first temperature of whose first derivative of absorbance is not zero to signify the onset of phase transition.

3.4. Results and Discussion

3.4.1. Results and Discussion for turbidity measurements of E3 and E1-80

Temperature-dependent turbidity profiles for two concentrations of both E3 and E1-80 under various heat power input are shown in Figure 7. Turbidity profiles are processed by a temperature-controlled UV-vis spectrophotometer, and described as absorbance as a function of temperature (scatter points with line). For each sample, we measure a logarithmic growth curve corresponding to the formation of coacervates as temperature is increased, which is consistent with previously reported phase transition behavior of ELP solutions[79]. For each sample turbidity profile, curves from left to right represent ramping speed 2 ˚C/min, 1 ˚C/min, 0.5 ˚C/min, 0.25 ˚C/min, and 0.1 ˚C/min respectively.

We can observe that for a high concentration 1mM for both E3 and E1-80, ramping speed has an observable effect on transition temperature (Tt), which implies that heat power input ($\frac{\partial Q}{\partial t}$) can shift the measured transition temperature required for detectable phase separation. Another key observation is that temperature ramp rate may

influence coacervate size distribution. For example, we observe a consistent trend of increased absorbance for increasing temperature ramp rate. Based on the hypothesis that large particles can scatter more light, large absorbance values, with maximum absorbance taken to be at the plateau of the turbidity curve imply the possibility of larger coacervate drops at the incipient stages of phase separation. Further work is needed to explore this hypothesis and the initial results presented herein lay the foundation for those investigations. Transition temperatures were predicted in python by Sigmodal curve fitting. Fitting results are shown in Figure 8; predicted transition temperatures are shown in Table 2.

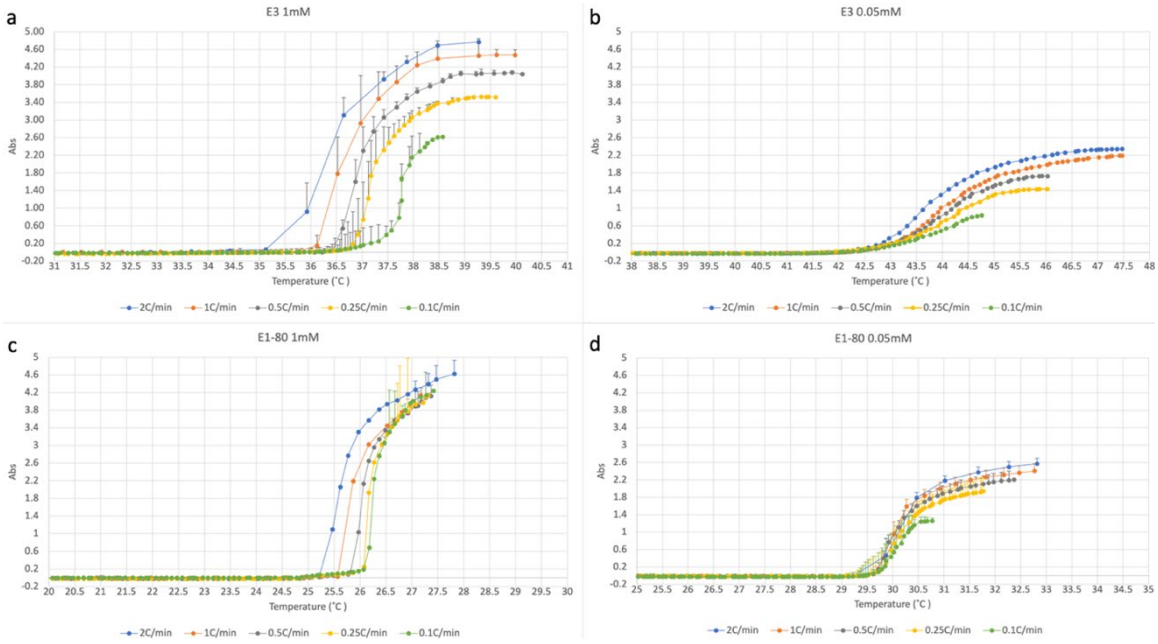

Figure 7 Absorbance measured as a function of temperature for (a) E3 at concentration 1mM, (b) E3 at concentration 0.05mM, (c) E1-80 at concentration 1mM, (d) E1-80 at concentration 0.05mM under virous heat input from large to small. Absorbance is plotted mean values plus standard deviations of nine measurements.

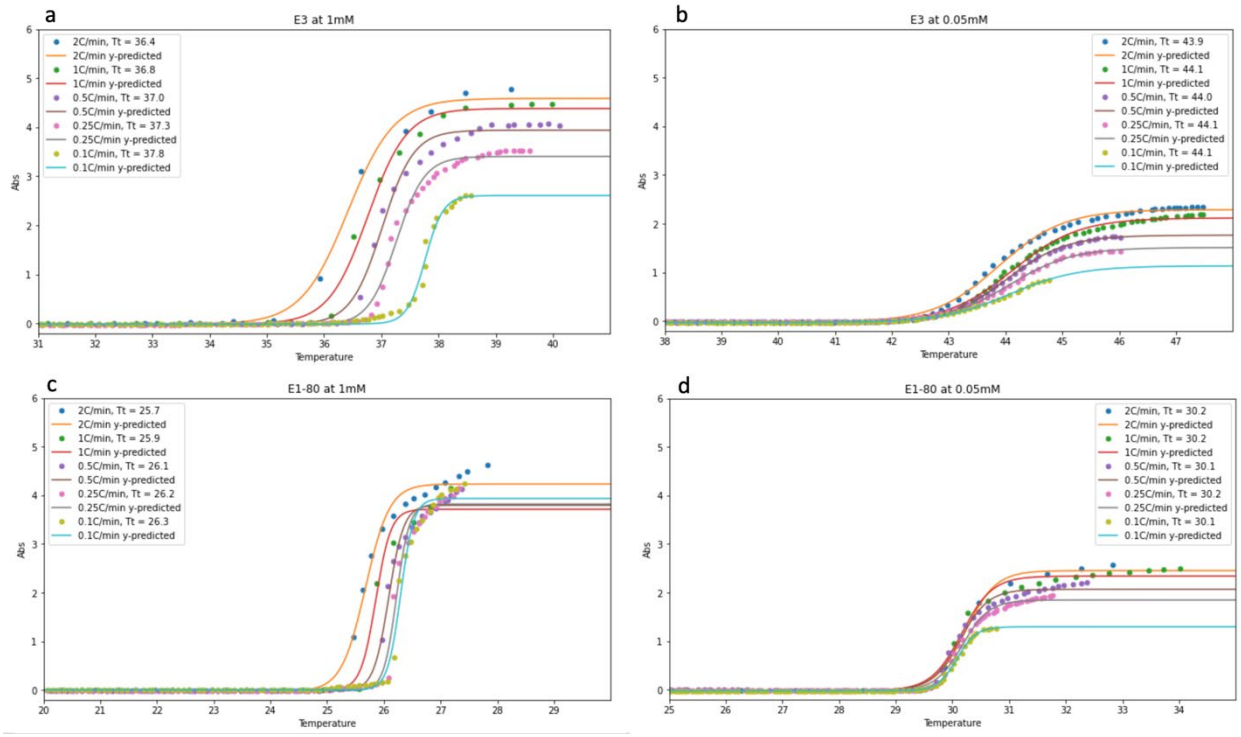

Figure 8 Sigmoidal curve fitting for (a) E3 at concentration 1mM, (b) E3 at concentration 0.05mM, (c) E1-80 at concentration 1mM, (d) E1-80 at concentration 0.05mM

Ramp Rate	Tt of E3 1mM	Tt of E3 0.05mM	Tt of E1-80 1mM	Tt of E1-80 0.05mM
2 ˚C/min	36.4 ˚C	43.9 ˚C	25.7 ˚C	30.2 ˚C
1 ˚C/min	36.8 ˚C	44.1 ˚C	25.9 ˚C	30.2 ˚C
0.5 ˚C/min	37.0 ˚C	44.0 ˚C	26.1 ˚C	30.1 ˚C
0.25 ˚C/min	37.3 ˚C	44.1 ˚C	26.2 ˚C	30.2 ˚C
0.1 ˚C/min	37.8 ˚C	44.1 ˚C	26.3 ˚C	30.1 ˚C

Table 2 Tt of E3 and E1-80 at concentration 1mM and 0.05mM respectively

Another observation, as evidenced by inspection of Table 2, is that for low concentrations of E1-80 and E3, there is little change in the measured Tt as a function of ramp rate. However, the Tt dependence on ramp rate for 1mM concentrations for both E1-80 and E3 are somewhat more pronounced with 1 ˚C and 0.6 ˚C difference between minimum (0.1 ˚C/min) and maximum (2 ˚C/min) ramp rates for E3 and E1-80, respectively. Our investigation also suggests a more pronounced dependence of Tt on

temperature ramp rate for the charged ELP E3 verses that of near neutrally charged E1-80. These measurements, with consistent trends, set the stage for future experimental and theoretical investigation of our system to elucidate the mechanisms behind the influence of temperature ramp rate and heat input on ionic and neutrally charged ELP (and other IDP) transition temperature and coacervate size distribution.

3.4.2. Limitations/Recommendations for future research

UV-vis spectrophotometer as an instrumentation to determine transition temperature at high concentration (more than 0.5mM) has its limitation of accurately detect the intensity of light passing through the sample if it is too weak. Once the absorbance passes five, there will be noise shown as 10 when the light intensity is too weak to be measured by the detector. This can be fixed by using cuvettes with shorter light pathlength to get a trustable absorbance or by using other techniques such as side scattering.

One other flaw of these turbidity measurements of various components is that they do not detail transformation of shape, size or growth mechanism in a phase separation. To be able to really understand the phase separation mechanism, microscopy equipped with temperature ramp apparatus should be used for separation process observation.

4. Chapter 4: Estimating Binodal Phase Boundary by Calculating Phase Volume Fractions in Capillaries Using Mass Balance Equation

This chapter describes a new method to construct a binodal curve in the phase diagram by measuring the amount of coacervate phase in a capillary followed by solving the mass balance equation.

4.1. Introduction

4.1.1. Synopsis

A binodal curve is a plot showing phase boundaries made of phases of different polymer compositions over a range of temperatures. It is critical to know the boundary between two phase and one phase region for a polymer solution as LLPS is an important physical property for any biopolymer application. We use the mass balance equation to derive an equation that describes the relationship among water-rich phase volume ratio, coacervate-rich phase volume ratio, water-rich phase volume fraction, and coacervate-rich phase volume fraction with given concentrations. Among these unknowns, the coacervate-rich and water-rich phase volume ratios are determined experimentally. ELPs at different concentration were added and sealed into capillaries for measurements of phase separation. Lengths of overall mixture and two phases are measured separately and used to solve the equation. The binodal curve was then constructed using water-rich and coacervate-rich phase volume fractions over a range of temperature.

4.2. Methods

4.2.1. Materials

PBS was purchased from Alfa Aesar (Ward Hill, MA). Isopropyl β-D-1-thiogalactopyranoside (IPTG) was purchased from Amresco Inc. (Solon, OH). Terrific broth media powder was purchased from MO BIO laboratories Inc. (Carlsbad, CA). Paroline oil was purchased from Sigma Aldrich (St. Louis, MO). Syringe pumps were purchased from Chemyx Inc. (Holliston, MA). Polyethylenimine (PEI) was purchased from Spectrum Inc. (New Brunswick, NJ). SDS-PAGE gel, Laemmli Sample Buffer, Coomassie Stains, SDS running buffer were purchased from Bio-Rad Laboratories Inc.

(Hercules, CA). Glass capillaries were purchased from The Lab Depot (Dawsonville, GA).

4.2.2. Procedures

4.2.2.1. Protein expression and purification of E1-80 and E3

Both E3 and E1-80 were expressed in E. coli BL21(DE3) cells and purified by ITC and then were characterized by SDS-PAGE gel as described in Chapter 3.

4.2.2.2. Volume Ratio between ELP-rich phase and water-rich phase at different temperatures with different concentrations

Aqueous solutions of E3 and E1-80 were prepared separately with buffer PBS at various concentrations from 0.5mM to 6mM. In a capillary, 75μL solution was added and sealed with wax clay and parafilm. When adding samples, care was taken to avoid having air bubbles in capillaries as air expansion upon temperature increase may increase the pressure. E4 capillaries were made in cold room to avoid phase transition. All capillaries with same type of ELP were then placed vertically in a preheated oven for phase separation. Temperature controlled centrifugation was used to accelerate coacervate settlement to the bottom of the capillaries, as phase separation could take up to 24 hours, during which time solution composition could change due to evaporation. The oven set temperature ranged from when at least two capillaries phase separated (most concentrated samples), with an interval of every two degrees, to approximately 50 ˚C where wax clay will melt. Photos were taken after the mixture separated into two macroscopically coexisting liquid phases with a clear meniscus (3-4hrs).

4.2.2.3. PEGylation of glass surface

It was observed that E1-80 coacervates exhibited pinning on the glass capillary walls while phase separating. Small drops would stick to capillary inner surface without releasing even after centrifugation. We used glass surface passivation with poly (ethylene glycol) silane (PEG-silane) to prevent pinning. Piranha solution was first used to clean the inner surface of capillaries during sonification. After rinsed with Milli-Q water for a few times, 0.5 M solution of NaOH was used in sonication to maximize the surface density of silanol groups. Water molecules were removed by soaking and washing in HPLC grade acetone for 5 min[80]. Capillaries were then dried under a nitrogen stream and were immersed in a 25% (w/w) solution of PEG-silane in dry DMSO for 20 min at 90 ˚C for PEG-coating. Capillaries were washed with water (Molecular Biology) and dried under nitrogen stream. PEGylated capillaries were then used as described in previous sections for phase separation.

4.3. Data Analysis

4.3.1. Phase Volume Fraction by solving Mass balance equation

For each of the ELP concentrations, after phase separation two distinct phase lengths were first measured by processing electronic photographs with the software ImageJ. The average length was taken after each measurement was measured three times. Phase volume ratios between V_{phase} and $V_{overall}$ were then calculated as $\frac{L_{phase}}{L_{overall}}$ given that cross-section diameters for two cylinders are same. From two phase volume ratios we estimate the ELP composition in two phases by solving the mass balance equation:

$$\emptyset_0 V_0 = \emptyset_L V_L + \emptyset_C V_C \,, \qquad (1)$$

where $\emptyset_0$, $\emptyset_L$, and $\emptyset_C$ are ELP compositions in the total solution, water-rich and coacervate-rich phases, respectively; V_0 , V_L , and V_C are volumes of the total solution, water-rich and coacervate-rich phases, respectively. The three terms in this equation represents the total amount of ELP in solution, the amounts of ELP in water-rich and coacervate-rich phases. Divide both sides of the equation by V_0, we get:

$$\emptyset_0 = \emptyset_L \frac{V_L}{V_0} + \emptyset_C \frac{V_C}{V_0} . \qquad (2)$$

$\emptyset_0$, total volume fraction, is defined as the volume of a polymer divided by the volume of all constituents of the mixture prior to mixing:

$$\emptyset_0 = \frac{V_{ELP}}{V_{ELP} + V_{buffer}} . \qquad (3)$$

Dividing the numerator and denominator of the right side of this equation by V_{buffer} , we get:

$$\emptyset_0 = \frac{\frac{V_{ELP}}{V_{buffer}}}{\frac{V_{ELP}}{V_{buffer}} + 1} . \qquad (4)$$

V_{ELP} can be calculated by ELP molar volume (ν_{ELP}) times the number of moles of ELP (n_{ELP}) in solution. Molar volume (ν_{ELP}) is equivalent to molar mass by ELP density. For ELP density, the aggregated phase usually contains up to ~60% water by weight (Urry et al. 1985), so it is here assumed the same as water ($\rho \approx 1$ g/cm^3). Value of volume fraction could be further investigated. $\frac{V_{ELP}}{V_{buffer}}$ can be estimated from:

$$\frac{V_{ELP}}{V_{buffer}} = \frac{\nu_{ELP}\, n_{ELP}}{V_{buffer}} , \qquad (5)$$

where $\frac{n_{ELP}}{V_{buffer}}$ is defined as the ELP concentration. We also have:

$$\frac{V_{ELP}}{V_{buffer}} = \nu_{ELP}\, C_{ELP} . \qquad (6)$$

Combine equation (6) and (4), we get:

$$\emptyset_0 = \frac{\nu_{ELP}\, C_{ELP}}{\nu_{ELP}\, C_{ELP} + 1}, \qquad (7)$$

Which is the equation between concentration and volume fraction in a ELP binary system.

Rearranging equation (2) and (7), we have:

$$\frac{\nu_{ELP}\, C_{ELP}}{\nu_{ELP}\, C_{ELP} + 1} = \emptyset_L \frac{V_L}{V_0} + \emptyset_C \frac{V_C}{V_0}, \qquad (8)$$

where concentration is preset, two phase volume ratios are measured and calculated from previous steps, ν_{ELP} is equivalent to molar mass by ELP density. Two sets of volume ratios of one concentration were used to solve equation (8) to be able to get water-rich and coacervate-rich phase volume fractions $\emptyset_L$ and $\emptyset_C$.

4.3.2. Plotting the binodal curve by using different compositions under different temperatures

Temperatures as function of ELP compositions in both phases were plotted and a spline function (from python) was used to depict the binodal curve.

4.4. Results and Discussion

4.4.1. Results and Discussion for E3

4.4.1.1. Presentation of results, data analysis and discussion

Photographs of E3 solutions in capillaries after phase separation at temperature 48˚C, 46˚C, 44˚C, 42˚C, 40 ˚C, and 39 ˚C are shown in Fig. 6 from left to right.

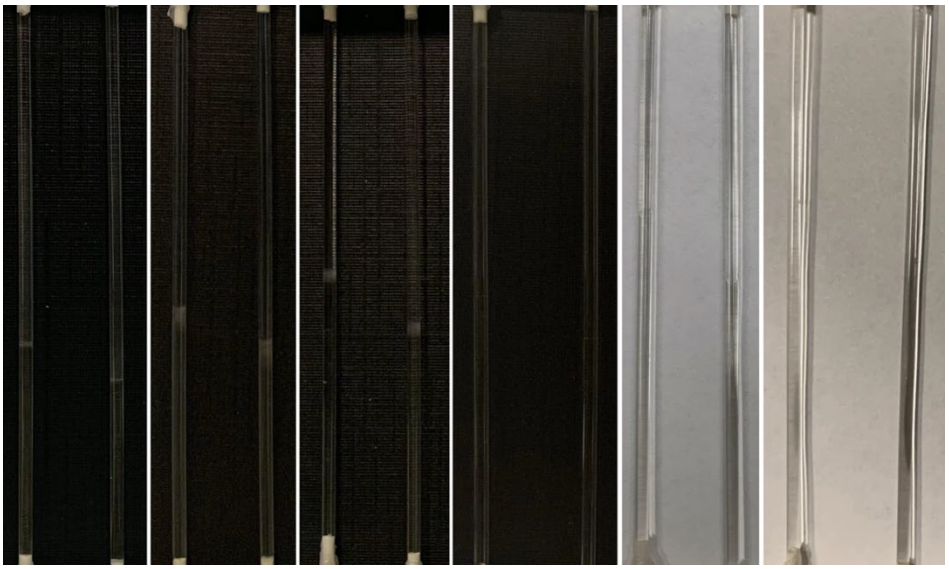

Figure 9 6mM and 5mM of E3 solution in clay wax sealed capillaries at temperatures 48˚C, 46˚C, 44˚C, 42˚C, 40 ˚C, and 39 ˚C

After measuring lengths of phases for initial solution concentrations 5mM and 6mM with ImageJ, volume ratios of two distinct phases separated by a sharp meniscus were calculated as shown in Table 3.

Temp.	Con.	Volume ratio water-rich	Volume ratio ELP-rich	Volume fraction water-rich	Volume fraction ELP-rich
48˚C	5mM	0.657	0.343	0.019	0.398
	6mM	0.592	0.408		
46˚C	5mM	0.603	0.397	0.022	0.343
	6mM	0.527	0.473		
44˚C	5mM	0.571	0.429	0.022	0.317
	6mM	0.487	0.513		
42˚C	5mM	0.558	0.412	0.027	0.303
	6mM	0.469	0.531		
40˚C	5mM	0.541	0.459	0.037	0.280
	6mM	0.439	0.561		
39˚C	5mM	0.527	0.473	0.041	0.268
	6mM	0.420	0.580		

Table 3 E3 Volume ratios and Volume fractions calculated for temperature 48˚C, 46˚C, 44˚C, 42˚C, 40 ˚C, and 39 ˚C using measurements from concentration 5mM and 6mM

By plotting temperatures as a function of volume fraction, the results are shown as Figure 10. As temperature decrease, volume fractions of both phases get closer. Missing data is because that at low temperature, the interface between phases becomes subtle and was hard to read.

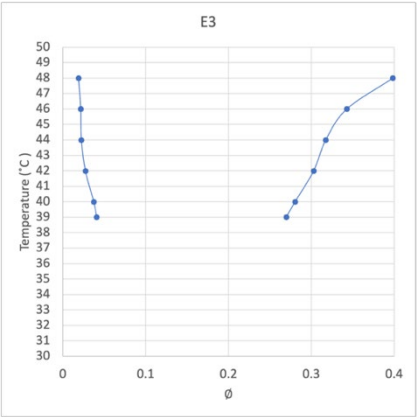

Figure 10 Temperature shown as a function of volume fraction for E3.

4.4.1.2. Comparison with binodal curve with the literature

Constructed binodal curve was then compared with another E3 binodal curve measured by dynamic light-scattering (DLS). The binodal curve constructed by capillary measurements looks more like a spinodal curve comparing to the one constructed by DLS. This could be related to insufficient incubation time. Further experiments may be needed to verify this hypothesis by incubation for a longer period of time.

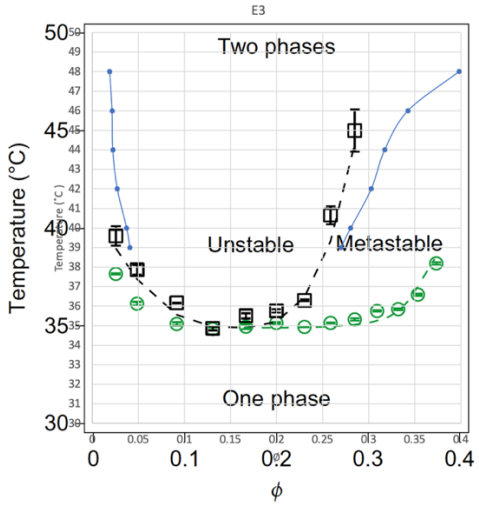

Figure 11 Overlayed binodal curves by capillary measurements and DLS. Figure adapted from[81].

4.4.2. PEGylation and issues with PEGylation for E1-80

E1-80 was observed to exhibit a pining phenomenon after phase separation at a relatively high temperature (42 ˚C). These small drops sticking to the inner surface could not be solved even after centrifugation. PEGylation was then used to passivation the inner surface of capillaries. As shown in Figure 12, after PEGylation, E1-80-rich droplets were able to be pulled down to the bottom by centrifugation. The turbidity of E1-80 stayed even after enough time of phase separation (4 days) could be related to special conformation formation.

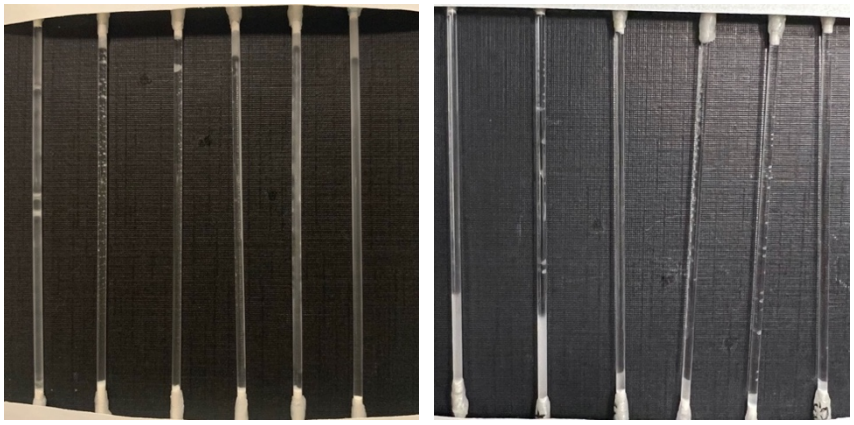

Figure 12 Before (left) and after (right) PEGylation of inner surface of capillaries

4.4.3. Limitations/Recommendations for future research

Capillary method for construction the whole binodal curve is limited by unclear interphase at low temperature, however, it could still be an easy way to determine higher branches of binodal or spinodal curve. In addition, this method requires high careful operation while making these capillaries to avoid air bubbles, and a relatively flat cross-section of the clay wax is required.

Reference:

[1] Abdolmaleki, M., Tavakoli, T., Jazani, O. M., & Saeb, M. R. (2016). Blend membranes based on polyurethane and polyethylene glycol: exploring the impact of molecular weight and concentration of the second phase on gas permeation enhancement. Journal of Polymer Engineering, 36(5), 513-519.

[2] Majumdar, A.; Dogra, P.; Maity, S.; Mukhopadhyay, S. Liquid-Liquid Phase Separation Is Driven by Large-Scale Conformational Unwinding and Fluctuations of Intrinsically Disordered Protein Molecules. J Phys Chem Lett 2019, 10, 3929–3936, doi: 10.1021/acs.jpclett.9b01731.

[3] Mao, H., Qiu, Z., Xie, B., Wang, Z., Shen, Z., & Hou, W. (2016, March). Development and application of ultra-high temperature drilling fluids in offshore oilfield around Bohai Sea bay basin, China. In *Offshore Technology Conference Asia*. OnePetro.

[4] Solec, K. (1970). Cloud-Point Curves of Polymer Solutions. Macromolecules, 3(5), 665-673.

[5] Clark, E. A., & Lipson, J. E. G. (2012). LCST and UCST behavior in polymer solutions and blends. Polymer, 53(2), 536-545.

[6] Barton, B. F., Graham, P. D., & McHugh, A. J. (1998). Dynamics of spinodal decomposition in polymer solutions near a glass transition. Macromolecules, 31(5), 1672-1679.

[7] Kuwahara, N., & Kubota, K. (1992). Spinodal decomposition in a polymer solution. Physical Review A, 45(10), 7385.

[8] Hashimoto, T., Itakura, M., & Hasegawa, H. (1986). Late stage spinodal decomposition of a binary polymer mixture. I. Critical test of dynamical scaling on scattering function. The Journal of chemical physics, 85(10), 6118-6128.

[9] Barton, B. F., Graham, P. D., & McHugh, A. J. (1998). Dynamics of spinodal decomposition in polymer solutions near a glass transition. Macromolecules, 31(5), 1672-1679.

[10] Dunker, A. K., Brown, C. J., Lawson, J. D., Iakoucheva, L. M., & Obradović, Z. (2002). Intrinsic disorder and protein function. Biochemistry, 41(21), 6573-6582.

[11] Zhou, J., Zhao, S., & Dunker, A. K. (2018). Intrinsically disordered proteins link alternative splicing and post-translational modifications to complex cell signaling and regulation. Journal of molecular biology, 430(16), 2342-2359.

[12] Dyson, H. J., & Wright, P. E. (2005). Intrinsically unstructured proteins and their functions. Nature reviews Molecular cell biology, 6(3), 197-208.

[13] Breydo, L., & Uversky, V. N. (2011). Role of metal ions in aggregation of intrinsically disordered proteins in neurodegenerative diseases. Metallomics, 3(11), 1163-1180.

[14] Van Der Lee, R., Buljan, M., Lang, B., Weatheritt, R. J., Daughdrill, G. W., Dunker, A. K., ... & Babu, M. M. (2014). Classification of intrinsically disordered regions and proteins. Chemical reviews, 114(13), 6589-6631.

[15] Martin, E. W., & Mittag, T. (2018). Relationship of sequence and phase separation in protein low-complexity regions. Biochemistry, 57(17), 2478-2487.

[16] Uversky, V. N., Oldfield, C. J., Midic, U., Xie, H., Xue, B., Vucetic, S., ... & Dunker, A. K. (2009). Unfoldomics of human diseases: linking protein intrinsic disorder with diseases. BMC genomics, 10(1), 1-17.

[17] Breydo, L., & Uversky, V. N. (2011). Role of metal ions in aggregation of intrinsically disordered proteins in neurodegenerative diseases. Metallomics, 3(11), 1163-1180.

[18] Ward, J. J., Sodhi, J. S., McGuffin, L. J., Buxton, B. F., & Jones, D. T. (2004). Prediction and functional analysis of native disorder in proteins from the three kingdoms of life. Journal of molecular biology, 337(3), 635-645.

[19] Dunker, A. K., Brown, C. J., Lawson, J. D., Iakoucheva, L. M., & Obradović, Z. (2002). Intrinsic disorder and protein function. Biochemistry, 41(21), 6573-6582.

[20] Dunker, A. K., Brown, C. J., Lawson, J. D., Iakoucheva, L. M., & Obradović, Z. (2002). Intrinsic disorder and protein function. Biochemistry, 41(21), 6573-6582.

[21] Yang, J., Zeng, Y., Liu, Y., Gao, M., Liu, S., Su, Z., & Huang, Y. (2020). Electrostatic interactions in molecular recognition of intrinsically disordered proteins. Journal of Biomolecular Structure and Dynamics, 38(16), 4883-4894.

[22] Babu, M. M., van der Lee, R., de Groot, N. S., & Gsponer, J. (2011). Intrinsically disordered proteins: regulation and disease. Current opinion in structural biology, 21(3), 432-440.

[23] Vucetic, S., Obradovic, Z., Vacic, V., Radivojac, P., Peng, K., Iakoucheva, L. M., ... & Dunker, A. K. (2005). DisProt: a database of protein disorder. *Bioinformatics*, *21*(1), 137-140.

[24] Dosztányi, Z., Csizmok, V., Tompa, P., & Simon, I. (2005). IUPred: web server for the prediction of intrinsically unstructured regions of proteins based on estimated energy content. *Bioinformatics*, *21*(16), 3433-3434.

[25] Oates, M. E., Romero, P., Ishida, T., Ghalwash, M., Mizianty, M. J., Xue, B., ... & Gough, J. (2012). D2P2: database of disordered protein predictions. Nucleic acids research, 41(D1), D508-D516.

[26] Sandberg, L. B., Soskel, N. T., & Leslie, J. G. (1981). Elastin structure, biosynthesis, and relation to disease states. New England Journal of Medicine, 304(10), 566-579.

[27] Kumashiro, K. K., Ho, J. P., Niemczura, W. P., & Keeley, F. W. (2006). Cooperativity between the hydrophobic and cross-linking domains of elastin. Journal of Biological Chemistry, 281(33), 23757-23765.

[28] Keeley, F. W., Bellingham, C. M., & Woodhouse, K. A. (2002). Elastin as a self–organizing biomaterial: use of recombinantly expressed human elastin polypeptides as a model for investigations of structure and self–assembly of elastin. Philosophical Transactions of the Royal Society of London. Series B: Biological Sciences, 357(1418), 185-189.

[29] Vrhovski, B., Jensen, S., & Weiss, A. S. (1997). Coacervation characteristics of recombinant human tropoelastin. European Journal of Biochemistry, 250(1), 92-98.

[30] Chilkoti, A., Christensen, T., & MacKay, J. A. (2006). Stimulus responsive elastin biopolymers: applications in medicine and biotechnology. Current opinion in chemical biology, 10(6), 652-657.

[31] Li, N. K., Quiroz, F. G., Hall, C. K., Chilkoti, A., & Yingling, Y. G. (2014). Molecular description of the LCST behavior of an elastin-like polypeptide. Biomacromolecules, 15(10), 3522-3530.

[32] Qin, G., Perez, P. M., Mills, C. E., & Olsen, B. D. (2016). Effect of ELP sequence and fusion protein design on concentrated solution self-assembly. Biomacromolecules, 17(3), 928-934.

[33] Rauscher, S., Baud, S., Miao, M., Keeley, F. W., & Pomes, R. (2006). Proline and glycine control protein self-organization into elastomeric or amyloid fibrils. *Structure*, *14*(11), 1667-1676.

[34] Chow, D., Nunalee, M. L., Lim, D. W., Simnick, A. J., & Chilkoti, A. (2008). Peptide-based biopolymers in biomedicine and biotechnology. Materials Science and Engineering: R: Reports, 62(4), 125-155.

[35] Li, N. K., Quiroz, F. G., Hall, C. K., Chilkoti, A., & Yingling, Y. G. (2014). Molecular description of the LCST behavior of an elastin-like polypeptide. Biomacromolecules, 15(10), 3522-3530.

[36] Aladini, F., Araman, C., & Becker, C. F. (2016). Chemical synthesis and characterization of elastin-like polypeptides (ELPs) with variable guest residues. Journal of Peptide Science, 22(5), 334-342.

[37] MacEwan, S. R., Hassouneh, W., & Chilkoti, A. (2014). Non-chromatographic purification of recombinant elastin-like polypeptides and their fusions with peptides and proteins from Escherichia coli. Journal of visualized experiments: JoVE, (88).

[38] Christensen, T., Hassouneh, W., Trabbic-Carlson, K., & Chilkoti, A. (2013). Predicting transition temperatures of elastin-like polypeptide fusion proteins. *Biomacromolecules*, *14*(5), 1514-1519.

[39] Urry, D. W. (1997). Physical chemistry of biological free energy transduction as demonstrated by elastic protein-based polymers. *The Journal of Physical Chemistry B*, *101*(51), 11007-11028.

[40] Simon, J. R., Carroll, N. J., Rubinstein, M., Chilkoti, A., & López, G. P. (2017). Programming molecular self-assembly of intrinsically disordered proteins containing sequences of low complexity. *Nature chemistry*, *9*(6), 509-515.

[41] Schäfer-Soenen, H., Moerkerke, R., Berghmans, H., Koningsveld, R., Dušek, K., & Šolc, K. (1997). Zero and off-zero critical concentrations in systems containing polydisperse polymers with very high molar masses. 2. The system water− poly (vinyl methyl ether). Macromolecules, 30(3), 410-416.

[42] Lin, D., & Huang, Y. (2010). A thermal analysis method to predict the complete phase diagram of drug–polymer solid dispersions. International journal of pharmaceutics, 399(1-2), 109-115.

[43] Schäfer-Soenen, H., Moerkerke, R., Berghmans, H., Koningsveld, R., Dušek, K., & Šolc, K. (1997). Zero and off-zero critical concentrations in systems containing polydisperse polymers with very high molar masses. 2. The system water− poly (vinyl methyl ether). Macromolecules, 30(3), 410-416.

[44] Vandeweerdt, P. Ph.D. Thesis, Leuven, 1993.

[45] Kurnik, I. S., Mussagy, C. U., Pereira, J. F., & Lopes, A. M. (2020). Amphiphilic copolymer aqueous solutions with cholinium ionic liquids as adjuvants: New insights into determination of binodal curves and phase-separation mechanisms. Journal of Molecular Liquids, 318, 114245.

[46] Bremer, A., Mittag, T., & Heymann, M. (2020). Microfluidic characterization of macromolecular liquid–liquid phase separation. *Lab on a Chip*, *20*(22), 4225-4234.

[47] Shim, J. U., Cristobal, G., Link, D. R., Thorsen, T., Jia, Y., Piattelli, K., & Fraden, S. (2007). Control and measurement of the phase behavior of aqueous solutions using microfluidics. *Journal of the American Chemical Society*, *129*(28), 8825-8835.

[48] Dzuricky, M., Rogers, B. A., Shahid, A., Cremer, P. S., & Chilkoti, A. (2020). De novo engineering of intracellular condensates using artificial disordered proteins. Nature chemistry, 12(9), 814-825.

[49] Dzuricky, M., Rogers, B. A., Shahid, A., Cremer, P. S., & Chilkoti, A. (2020). De novo engineering of intracellular condensates using artificial disordered proteins. Nature chemistry, 12(9), 814-825.

[50] Dzuricky, M., Rogers, B. A., Shahid, A., Cremer, P. S., & Chilkoti, A. (2020). De novo engineering of intracellular condensates using artificial disordered proteins. Nature chemistry, 12(9), 814-825.

[51] Nott, T. J., Petsalaki, E., Farber, P., Jervis, D., Fussner, E., Plochowietz, A., ... & Baldwin, A. J. (2015). Phase transition of a disordered nuage protein generates environmentally responsive membraneless organelles. *Molecular cell*, *57*(5), 936-947.

[52] Nott, T. J., Petsalaki, E., Farber, P., Jervis, D., Fussner, E., Plochowietz, A., ... & Baldwin, A. J. (2015). Phase transition of a disordered nuage protein generates environmentally responsive membraneless organelles. *Molecular cell*, *57*(5), 936-947.

[53] Le Ferrand, H., Duchamp, M., Gabryelczyk, B., Cai, H., & Miserez, A. (2019). Time-resolved observations of liquid–liquid phase separation at the nanoscale using in situ

liquid transmission electron microscopy. *Journal of the American Chemical Society*, *141*(17), 7202-7210.

[54] Simon, J. R., Carroll, N. J., Rubinstein, M., Chilkoti, A., & López, G. P. (2017). Programming molecular self-assembly of intrinsically disordered proteins containing sequences of low complexity. *Nature chemistry*, *9*(6), 509-515.

[55] Simon, J. R., Carroll, N. J., Rubinstein, M., Chilkoti, A., & López, G. P. (2017). Programming molecular self-assembly of intrinsically disordered proteins containing sequences of low complexity. *Nature chemistry*, *9*(6), 509-515.

[56] Dzuricky, M., Rogers, B. A., Shahid, A., Cremer, P. S., & Chilkoti, A. (2020). De novo engineering of intracellular condensates using artificial disordered proteins. *Nature chemistry*, *12*(9), 814-825.

[57] Simon, J. R., Carroll, N. J., Rubinstein, M., Chilkoti, A., & López, G. P. (2017). Programming molecular self-assembly of intrinsically disordered proteins containing sequences of low complexity. *Nature chemistry*, *9*(6), 509-515.

[58] McDaniel, J. R., Radford, D. C., & Chilkoti, A. (2013). A unified model for de novo design of elastin-like polypeptides with tunable inverse transition temperatures. *Biomacromolecules*, *14*(8), 2866-2872.)

[59] Meyer, D. E., & Chilkoti, A. (1999). Purification of recombinant proteins by fusion with thermally-responsive polypeptides. *Nature biotechnology*, *17*(11), 1112-1115.

[60] Chilkoti, A., Dreher, M. R., Meyer, D. E., & Raucher, D. (2002). Targeted drug delivery by thermally responsive polymers. *Advanced drug delivery reviews*, *54*(5), 613-630.)

[61] Meyer, D. E., Trabbic-Carlson, K., & Chilkoti, A. (2001). Protein purification by fusion with an environmentally responsive elastin-like polypeptide: effect of polypeptide length on the purification of thioredoxin. *Biotechnology Progress*, *17*(4), 720-728.

[62] Meyer, D. E., & Chilkoti, A. (2002). Genetically encoded synthesis of protein-based polymers with precisely specified molecular weight and sequence by recursive directional ligation: examples from the elastin-like polypeptide system. *Biomacromolecules*, *3*(2), 357-367.

[63] Schuster, B. S., Reed, E. H., Parthasarathy, R., Jahnke, C. N., Caldwell, R. M., Bermudez, J. G., ... & Hammer, D. A. (2018). Controllable protein phase separation and

modular recruitment to form responsive membraneless organelles. *Nature communications*, *9*(1), 1-12.

[64] Fong, B. A., Wu, W. Y., & Wood, D. W. (2009). Optimization of ELP-intein mediated protein purification by salt substitution. *Protein expression and purification*, *66*(2), 198-202.

[65] Hartzell, E. J., Lieser, R. M., Sullivan, M. O., & Chen, W. (2020). Modular hepatitis B virus-like particle platform for biosensing and drug delivery. *ACS nano*, *14*(10), 12642-12651.

[66] McDaniel, J. R., Callahan, D. J., & Chilkoti, A. (2010). Drug delivery to solid tumors by elastin-like polypeptides. *Advanced drug delivery reviews*, *62*(15), 1456-1467.

[67] Nettles, D. L., Chilkoti, A., & Setton, L. A. (2010). Applications of elastin-like polypeptides in tissue engineering. *Advanced drug delivery reviews*, *62*(15), 1479-1485.

[68] Trabbic-Carlson, K., Liu, L., Kim, B., & Chilkoti, A. (2004). Expression and purification of recombinant proteins from Escherichia coli: Comparison of an elastin-like polypeptide fusion with an oligohistidine fusion. Protein Science, 13(12), 3274-3284.

[69] Loyez, M., Ribaut, C., Caucheteur, C., & Wattiez, R. (2019). Functionalized gold electroless-plated optical fiber gratings for reliable surface biosensing. Sensors and Actuators B: Chemical, 280, 54-61.

[70] Massodi, I., Bidwell III, G. L., & Raucher, D. (2005). Evaluation of cell penetrating peptides fused to elastin-like polypeptide for drug delivery. *Journal of controlled release*, *108*(2-3), 396-408.

[71] MacEwan, S. R., & Chilkoti, A. (2014). Applications of elastin-like polypeptides in drug delivery. Journal of Controlled Release, 190, 314-330.

[72] Betre, H., Setton, L. A., Meyer, D. E., & Chilkoti, A. (2002). Characterization of a genetically engineered elastin-like polypeptide for cartilaginous tissue repair. Biomacromolecules, 3(5), 910-916.

[73] Devalliere, J., Dooley, K., Hu, Y., Kelangi, S. S., Uygun, B. E., & Yarmush, M. L. (2017). Co-delivery of a growth factor and a tissue-protective molecule using elastin biopolymers accelerates wound healing in diabetic mice. Biomaterials, 141, 149-160.

[74] Adeeyinwo, C. E., Okorie, N. N., & Idowu, G. O. (2013). Basic calibration of UV/visible spectrophotometer. International Journal of Science and Technology, 2(3), 247-251.

[75] Brown, C. W. (2000). Ultraviolet, visible, and near-infrared spectrophotometers. Applied Spectroscopy Reviews, 35(3), 151-173.

[76] Dreher, M. R., Raucher, D., Balu, N., Colvin, O. M., Ludeman, S. M., & Chilkoti, A. (2003). Evaluation of an elastin-like polypeptide–doxorubicin conjugate for cancer therapy. *Journal of controlled release*, *91*(1-2), 31-43.

[77] Nath, N., & Chilkoti, A. (2001). Interfacial phase transition of an environmentally responsive elastin biopolymer adsorbed on functionalized gold nanoparticles studied by colloidal surface plasmon resonance. *Journal of the American Chemical Society*, *123*(34), 8197-8202.

[78] Compton, S. J., & Jones, C. G. Mechanism of dye response and interference in the Bradford protein assay. Anal Biochem. 151, 369-374, doi:10.1016/0003-2697(85)90190-3 (1985).

[79] Christensen, T., Hassouneh, W., Trabbic-Carlson, K., & Chilkoti, A. (2013). Predicting transition temperatures of elastin-like polypeptide fusion proteins. *Biomacromolecules*, *14*(5), 1514-1519.

[80] Gidi, Y., Bayram, S., Ablenas, C. J., Blum, A. S., & Cosa, G. (2018). Efficient one-step PEG-silane passivation of glass surfaces for single-molecule fluorescence studies. *ACS applied materials & interfaces*, *10*(46), 39505-39511.

[81] Simon, J. R., Carroll, N. J., Rubinstein, M., Chilkoti, A., & López, G. P. (2017). Programming molecular self-assembly of intrinsically disordered proteins containing sequences of low complexity. *Nature Chemistry*, *9*(6), 509-515.